VII International Conference on Particle-Based Methods
PARTICLES 2021
P. Wriggers, M. Bischoff, E. Oñate, A. Düster & T. Zohdi (Eds)

MODELLING OF THE DUST RELEASE FROM BULK SOLIDS IN THE EVENT OF PARTICLE IMPACT THROUGH ENHANCED DUST DETACHMENT FUNCTIONS

D. SCHULZ*[1], M. KAUL[2], G. REZNIK[2], E. SCHMIDT[2] AND H. KRUGGEL-EMDEN[1]

[1] Chair of Mechanical Process Engineering and Solids Processing
Technische Universität Berlin
Ernst-Reuter-Platz 1, D-10587 Berlin, Germany
E-mail: daniel.schulz@tu-berlin.de, Web page: https://www.mvta.tu-berlin.de/

[2] Institute of Particle Technology
University of Wuppertal
Rainer-Gruenter-Str, Geb. FF, D-42119 Wuppertal, Germany
Web page: https://www.ipt.uni-wuppertal.de/

Key words: Discrete Element Method (DEM), dust detachment functions, dust modelling, adhesive contacts

Summary. The detachment of fine adhered powder particles in the course of bulk particle-wall contacts is studied with a numerical Discrete Element Method (DEM). The model relies on an adhesive DEM to describe the carrier and the individual dust particle motion. Further, dust detachment functions are modified in a non-adhesive DEM method, in which only the coarse carrier particles are tracked as one composed bulk particle. The realized dust release functions include a normal and a tangential lift-off condition. Both dust release functions are benchmarked based on dust-resolved adhesive DEM simulations by varying the restitution coefficient and the impact angle in the event of bulk particle-wall contacts. The normal and the tangential lift-off conditions both reflect the physical detachment of individual dust particles very well assuming fine particles of constant size. The application of the enhanced dust detachment functions therefore allows to predict dust release of individual dust particles with significantly less computing time.

1 INTRODUCTION

Regarding environmental, health and explosion protection, it is of the utmost importance to assess the extent of diffuse dust emissions from bulk solids in advance. Additional to standardized dustiness tests and measurements under field conditions on real dust emissions, numerical methods such as the Discrete Element Method (DEM) coupled to Computational Fluid Dynamics (CFD) are promising approaches for the prediction of the latter [1]. Thereby, the DEM is suitable for modelling the motion of the individual bulk solid particles and the CFD to calculate the flow parameters of the gas phase, which is responsible for the resuspension of airborne dust particles. The latter dust particles are usually not modelled in detail due to computing time restrictions, but rather the detachment is described using so-called dust detachment functions. In order to model the dust spread supplementary to the detachment, the

dust phase can e.g. be modelled as a second granular fluid phase with an Eulerian-Eulerian approach [2] or by utilizing an Eulerian dust density field [3]. Approaches for describing the dust dispersion in the event of a particle impact are e.g. the particle-based approach by Cui and Sommerfeld [4] including a direct lift-off, a sliding and a rolling condition or the macroscopic dust detachment terms based on an energy formulation by Hilton and Cleary [3], which have to be calibrated based on a dustiness factor. Overall, there are only a few models that make it possible to predict the dust detachment in a DEM simulation without simulating each individual fine particle attached in detail. To close this gap, in our study dust detachment functions are further developed based on a benchmarking with dust-resolved adhesive DEM simulations, in which the individual fine particles are attached with an adhesive Johnson, Kendall, Roberts (JKR) [5] contact model. The enhanced dust detachment model based on single particle impacts includes a lift-off condition in normal direction [4] and a condition for tangential lift-off. Both criteria are validated for a bulk solid particle impact on a rigid wall under variation of the impact velocity and the impact angle.

2 SIMULATION METHOD

A Lagrangian DEM approach was used to model the bulk solid particles, which consist of carrier particles to which fine powder (dust) particles adhere. For both spherical carrier and dust particles, the translational and rotational motion can be obtained by integrating the Newton's and Euler's equations given by

$$m_i \frac{d^2\vec{x}_i}{dt^2} = \vec{F}_i^c + \vec{F}_i^{vdw} + m_i\vec{g}, \tag{1}$$

$$I_i \frac{d^2\vec{\varphi}_i}{dt^2} = \vec{M}_i,$$

with the particle mass m_i, the particle acceleration $d^2\vec{x}_i/dt^2$, the contact force $\vec{F}_i^c = \vec{F}_i^n + \vec{F}_i^t$ comprising of a normal $\vec{F}_i^n$ and a tangential component $\vec{F}_i^t$, the contactless van-der-Waals force $\vec{F}_i^{vdw}$, the gravitational force $m_i\vec{g}$, the angular acceleration $d^2\vec{\varphi}_i/dt^2$, the external moment $\vec{M}_i$ resulting out of particle contact forces and the moment of inertia I_i. Currently, any fluid dynamic effects were disregarded to simplify the modelling of the detachment process resulting from the bulk solid particle impact. Two types of DEM simulations were performed. In the first, all individual dust particles are tracked separately, while in the second only a single carrier particle impact alongside dust detachment functions is solved. The additional influence of adhesion is only present for contacts in which fine dust particles are involved. Consequently, the contactless van-der-Waals force $\vec{F}_i^{vdw}$ is neglected for the non-adhesive contacts. Therefore, only for non-existing fine particle contacts the adhesive van-der-Waals force $\vec{F}_i^{vdw}$ is calculated. It is dependent on the distance z between the contact partners by $F_i^{vdw} = A_{12}R_{12}/6z^2$ according to Hamaker [6] with A being the Hamaker constant. $\vec{F}_i^{vdw}$ is acting until the critical pull-off force $\vec{F}_c = 3\pi\gamma_{12}R_{12}$ of the JKR theory [5] is reached at the separation distance z_0. The pull-off force is obtained with the effective surface energy γ_{12} and the effective particle radius R_{12}. For non-adhesive contacts, the normal component of the contact force is derived from a non-linear contact model according to Tsuji et al. [7], which is based on the Hertz theory. For the calculation of the non-adhesive tangential forces, a classic linear spring is used according to

Mindlin [8] that is limited by the Coulomb condition with $\mu_c|F_i^n|$ as a critical sliding criterion. For adhesive dust particle contacts, the elastic component of the normal force F_i^{ne} is replaced by an elastic-adhesive force according to Chokshi et al. [9], who converted the equations of the JKR theory for usage in the DEM. Furthermore, the critical Coulomb condition of the tangential component is also adapted due to adhesive effects according to Thornton [10] and Thornton and Yin [11], who proposed a critical sliding criterion $\mu_f|F_i^{ne} + 2F_c|$ in the presence of adhesion. Supplementary, rolling friction is considered when adhesive dust particles are present, because contrary to the carrier particle-wall contacts significantly longer contact times occur due to the adhesive sticking of the fine particles on the carrier surface. The adhesive JKR-based rolling resistance model derived by Dominik und Tielens [12] is utilized, given by $M_i^r = -4F_c(a/a_0)^{3/2}\xi^r$, where a describes the contact radius and a_0 is the equilibrium contact radius both known from the underlying elastic-adhesive contact model. ξ^r describes the rolling displacement until the critical displacement $\xi_{crit}^r = R_{12}\theta_{crit}$ is reached corresponding to a critical rolling angle θ_{crit}.

3 NUMERICAL SETUP AND MATERIALS

Bulk solid particles according to a so-called reference test bulk material are considered as utilized before by Woschny et al. [13], who compared macroscopic dust release to numerical DEM/CFD simulations in a rotating drum apparatus and a wind tunnel. The test bulk material consists of a reproducible mixture with defined mass ratios of spherical particles (stainless steel) with a diameter of d_p = 0.0015 m and a density of ρ_p = 7700 kg/m³ along with adhesive attached fine powder particles (calcium carbonate) with a density of ρ_d = 2700 kg/m³ and a median distribution value of $x_{50,3}$ = 20 µm. Blends of both components were produced in a 3D-shaker mixer, whereby the powder was dried prior to processing to avoid any negative effect of capillary forces. For the reference test bulk material, the calcium carbonate powder represents the maximum available dust mass.

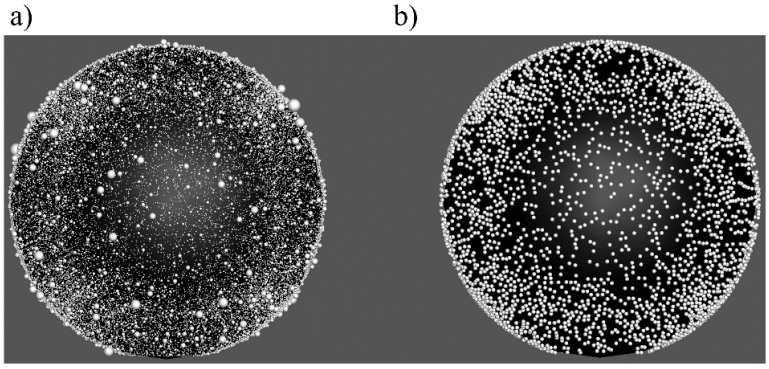

Figure 1: DEM visualization of attached dust particles adhering on the carrier particle for a) an exemplary particle distribution with a median distribution value of $x_{50,3}$ = 15 µm and b) an ideal adhering mean dust particle size of d_d = 20 µm both with a degree of dust coverage of X_0 = 20 %.

Current investigations indicate that the particle distributions can slightly decrease after mixing, which is visualized in Fig. 1a) for an exemplary bulk particle with an adhered particle mean size distribution value of $x_{50,3}$ = 15 µm and a degree of dust coverage of X_0 = 20 %, which

fits well with current experimental observations. The degree of dust coverage X_0 indicates thereby the ratio of the summarized cross-section area of all adhering fine particles to the bulk solid particle surface. As a first step to examine the detachment process in a simplified manner, in this study a monolayer of powder particles with a constant fine particle diameter of d_d = 20 µm and X_0 = 20 % was investigated in the DEM simulations (see Fig. 1b)). To simplify the collision process in the DEM, for the generation of the randomly distributed monolayer no dust particles are present in the area of carrier impact with the wall. The values for the Hamaker constants were estimated and set to $A_{dd} = 10.1 \cdot 10^{-20}$ for the powder particles according to calculations performed using the full Lifshitz theory [14] and to $A_{pp} = 21.2 \cdot 10^{-20}$ according to surface tension measurements of iron [15]. The Hamaker constant for the adhesion of the powder particles on the carrier particle is given by the geometric mean $A_{12} = \sqrt{A_{11}A_{22}}$. The surface energy γ_{pd} required for the used adhesive JKR-based contact model was therefore fitted with the balance of the pull-off force F_c and the van-der-Waals force at the separation distance z_0 with $\gamma_{12} = A_{12}/(18\pi z_0^2)$. A time step of 10^{-9} s was used in all simulations so that the contacts are resolved with sufficient precision. Gravitation is neglected in the DEM simulations, so the impact velocity and the contact angle can be defined with an initial velocity vector.

3 NUMERICAL SETUP AND MATERIALS

In the following, straight and oblique impacts on a rigid wall are examined using the above-described adhesive DEM-JKR model. In addition to the dust-resolved simulations, DEM simulations without adhering dust particles are performed. Instead, it is relied on dust release functions that calculate the dust detachment based on the forces acting on the carrier particle. The restitution coefficient between the carrier particle and the wall is varied for the straight, vertical impact as well as the impact angle is varied for the straight/oblique impact.

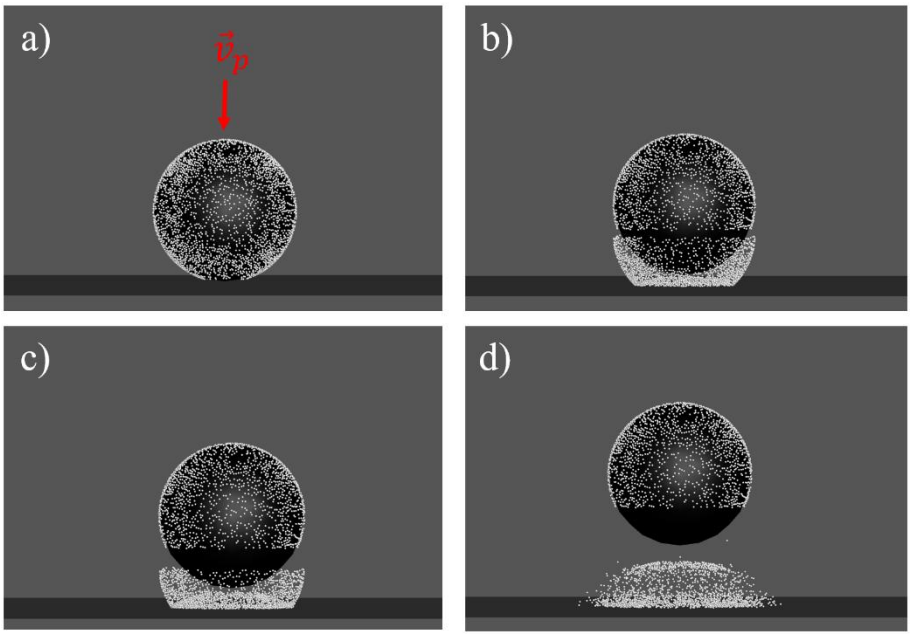

Figure 2: Exemplary visualization of a dust-resolved DEM simulation showing a straight, vertical bulk particle-wall impact with v_p = 4 m/s a) just before the impact and (b-d) after the rebound.

3.1 Improvement of the particle-based dust detachment model

In Fig. 2 and in Fig. 3 exemplary dust-resolved impacts of bulk solid particles are visualized. The subpicture a) shows the bulk particle shortly before the impact, the subpictures (b-c) shortly after the impact and d) at a later point in time after the rebound. The first scenario in Fig. 2 shows a straight impact (α = 90°) with an impact velocity of v_p = 4 m/s and the second scenario in Fig. 3 an oblique impact with an impact angle of α = 60° and an impact velocity of v_p = 12 m/s. Thereby, the impact angle α denotes the angle between the initial velocity vector and the wall orientation (see Fig. 3a)). The first scenario demonstrates that at a lower impact velocity only dust particles located on the southern hemisphere are detached assuming a constant adhering dust particle size. The southern hemisphere refers to the hemisphere of the carrier surface on which the point of impact is located.

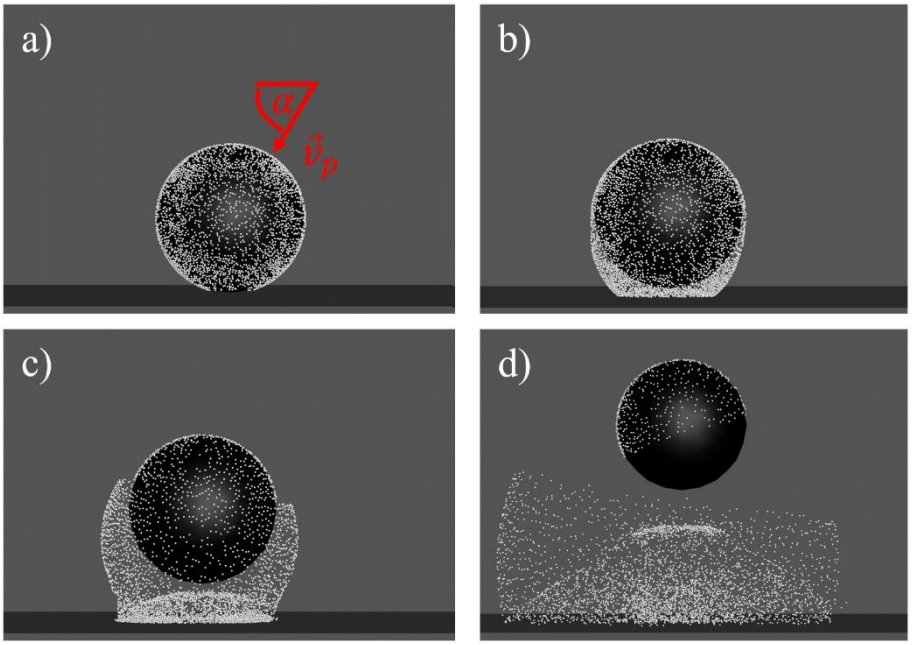

Figure 3: Exemplary visualization of a dust-resolved DEM simulation showing an oblique bulk particle-wall impact with v_p= 12 m/s and α = 60° a) just before the impact and (b-d) after the rebound.

With higher inertia forces (see Fig. 3b)), dust particles are also thrown off from the northern hemisphere, which is the carrier particle surface opposite the point of impact. It can be observed, that dust particles not detached from the northern hemisphere tend to slide and roll a certain distance towards the point of impact until they adhere again without slippage. For the used adhesive contact models in the DEM, the unknown coefficient of friction μ_f and the critical rolling angle θ_{crit} of the adhesive dust particles must be specified. In the performed simulations, it is assumed that the dust particles only slide a short distance before they adhere again without slippage or detachment. Therefore, the coefficient of friction was set to μ_f = 0.3 and the critical rolling angle to θ_{crit} = 0.15, so that only direct lift-off from the particles located on the northern hemisphere can be observed shortly after the bulk solid has rebounded. Preliminary investigations have shown that the critical rolling angle θ_{crit} has no influence on the dust

detachment, except when it is set to low values that result in dust particle collisions. In contrast, the coefficient of friction can influence the detachment, since depending on its value more kinetic energy is dissipated of the stressed dust particles. It should be noted, that due to the constant adhered powder particle size, the effect of dust particle contacts on the carrier surface is almost excluded.

Ibrahim et al. [16] established three particle-based dust detachment modes for micro particle detachment from surfaces by air flow, including a direct lift-off, a sliding and a rolling condition. They determined rolling as the primary detachment mechanism for sparse monolayers. Cui et al. [4] applied similar detachment criteria in a Lagrangian particle tracking algorithm to predict drug detachment probability within an inhaler device via wall collisions depending on the acting forces of inertia. Adapted to our implemented critical sliding condition of the dust particles, the lift-off, sliding and rolling criteria for each contact DEM time step are given by

$$\textit{Lift-off:} \quad F_{in,d}^{n} > F_c, \tag{2}$$

$$\textit{Sliding:} \quad F_{in,d}^{t} > \mu_f \left| 2F_c - F_{in,d}^{n} \right|,$$

$$\textit{Rolling:} \quad F_{in,d}^{t} R_d > \left| F_c - F_{in,d}^{n} \right| a_0,$$

where $F_{in,d}^{n}$ and $F_{in,d}^{t}$ are the inertia forces acting on the individual adhered dust particle in normal and tangential direction, F_c denotes the pull-off force, R_d is the radius of the dust particle and a_0 is the equilibrium contact radius known from the underlying JKR-theory. Both of the inertia forces can be converted with known fixed positions of the adhered dust particles and based on the mass ratios of carrier and dust particle. The direct lift-off in the normal direction can only take place on the southern hemisphere, because on the northern hemisphere the inertia force is acting in the same direction as the pull-off force F_c.

Looking at our dust-resolved DEM-JKR simulations, both sliding and rolling motion on the carrier particle surface are present, but both do not yet mean detachment. Opposite to a constant stress by an air flow, the dust particles are only stressed for a short time after impact and can stick again without slippage after a short sliding and rolling period. Therefore, only the lift-off condition from Eqn. 2 is used for the southern hemisphere, which is referred to in the following as normal lift-off condition. Furthermore, for the northern hemisphere an additional tangential lift-off condition is introduced as a second detachment criterion.

The individual attached dust particles on the northern hemisphere always detach shortly after the rebound in the event of bulk particle-wall impacts. If the adhesive force is strong enough to keep the dust particles attached, they can slide on the surface until they stick again without slippage. Immediate after the rebound, the dust particles slide with a relative translational velocity $v_{t,rel}$ on the carrier surface towards the impact point. In this case, the pull-off force acts as a centripetal force to keep the dust particle on the curved path. However, the dust particle can also detach in tangential direction if a critical velocity is exceeded. The apparent centrifugal force resulting from the dust particle motion is directed opposite to the pull-off force and can be described with $m_d v_{t,rel}^2 / \left\| r_{pd} \right\|$, where r_{pd} is the sum of the radii of both contact partners. Thus, in addition to the normal lift-off condition, a tangential lift-off condition is added, which leads to our modified dust detachment model

Lift-off-normal: $F_{in,d}^{n} > F_c$, (3)

Lift-off-tangential: $\frac{m_d v_{t,rel}^2}{\|r_{pd}\|} > F_c$.

To solve the tangential condition, the translational relative velocity $v_{t,rel}$ between the dust and the carrier particle immediate after the rebound is required. We define the position vector of the individual adhered dust particle as $\vec{r}_{pd} = \vec{x}_d - \vec{x}_p$, with the position of the dust particle center $\vec{x}_d$ and the position of the carrier particle center $\vec{x}_p$. Thus, $v_{t,rel}$ at the carrier rebound can be estimated for each dust particle without the influence of friction by

$$\vec{v}_{t,rel\ (without\ friction)} = \Delta\vec{v}_p - \frac{\vec{r}_{pd} \cdot \Delta\vec{v}_p}{\|\vec{r}_{pd}\|}, \tag{4}$$

with the relative carrier velocity $\Delta\vec{v}_p = \vec{v}_{contact} - \vec{v}_{rebound}$ determined from the impact velocity at first contact and the rebound velocity when the carrier particle no longer overlaps with the wall. Furthermore, for the estimation of the frictional energy that slows down the dust particle during the carrier-wall contact an optional friction term is introduced.

In the following, a methodology is shown to roughly estimate the frictional energy that acts during contact, without simulating each dust particle with the DEM in detail. $\vec{v}_{t,rel}$ is therefore estimated with the dust particle mass m_d and with the difference in the kinetic energy E_{kin}^{t} without the influence of friction minus the estimated friction work $E_{friction}^{t}$ as follows

$$v_{t,rel} = \sqrt{\frac{2(E_{kin\ (without\ friction)}^{t} - E_{friction}^{t})}{m_d}}, \tag{5}$$

$$E_{kin\ (without\ friction)}^{t} = \frac{1}{2} m_d v_{t,rel\ (without\ friction)}^2.$$

The frictional work is the integral of the frictional tangential force F^t over the translational displacement ξ^d. Since the tangential force F^t between the carrier and the dust particle is not known in the dust-unresolved DEM, $E_{friction}^{t}$ can only be estimated with an average tangential force $\bar{F}^t$. As a first step, we estimate the translational displacement ξ^d of the dust particle on the carrier surface during the carrier contact to increase linearly over the contact time $\Delta t_{pw,contact}$. Further, as a second estimation, we approximate $\bar{F}^t$ with ½ of the maximum tangential force $F_{max,d}^{t}$, which can be determined for each dust particle using the sliding condition (compare Eqn. (2)) as the maximum inertia force in tangential direction. This leads to

$$E_{friction}^{t} = \int_0^{\xi^d} F^t \, d\xi^d \sim \bar{F}^t \xi^t, \tag{6}$$

$$\xi^d \sim \frac{1}{2} v_{t,rel\ (without\ friction)} \Delta t_{pw,contact},$$

$$\bar{F}^t = \frac{1}{2} F_{max,d}^{t} = \frac{1}{2} \mu_f \, max\left(\left|F_{in,d}^{n} + 2F_c\right|\right).$$

Eqn. (4-6) were accordingly realized in the dust-unresolved DEM. The comparison of the overall dust detachment between the dust-resolved adhesive DEM-JKR model and the application of the simpler dust detachment functions (Eqn. (4-6)) is discussed in the next subsection.

3.2 Benchmarking of the enhanced dust detachment functions for particle-wall impacts

Straight, vertical bulk particle-wall impacts by varying the restitution coefficient e_{pw} of the carrier particle and straight/oblique impacts by varying the impact angle α are investigated for the benchmarking of the modified dust detachment model. All simulations were carried out for a sufficiently long time until no further relative motion of the carrier and dust particles was observed and these adhere without slippage. In Fig. 4, the dispersion ratio of both adhesive DEM-JKR simulations and as a consequence of the application of the dust release functions in the DEM is presented. We thereby define the dispersion ratio as the mass ratio of detached dust particles to the initial layer of dust particles. It is visible that the dust particles on the southern hemisphere are almost completely detached up to an impact velocity of v_p = 2-4 m/s (dispersion ratio = 50 %). From an impact velocity of 6 m/s or higher, the particles on the northern hemisphere which move towards the carrier during impact also start to detach in tangential direction. On both hemispheres, a good match with the dust release functions is made. The influence of the restitution coefficient is hardly noticeable on the southern hemisphere, as the maximum acting inertia force is similar during the impacts. On the northern hemisphere, a lower restitution coefficient (e_{pw} = 0.5) leads to more energy dissipation, which also affects the tangential energy of the dust particles and leads to less dust dispersion.

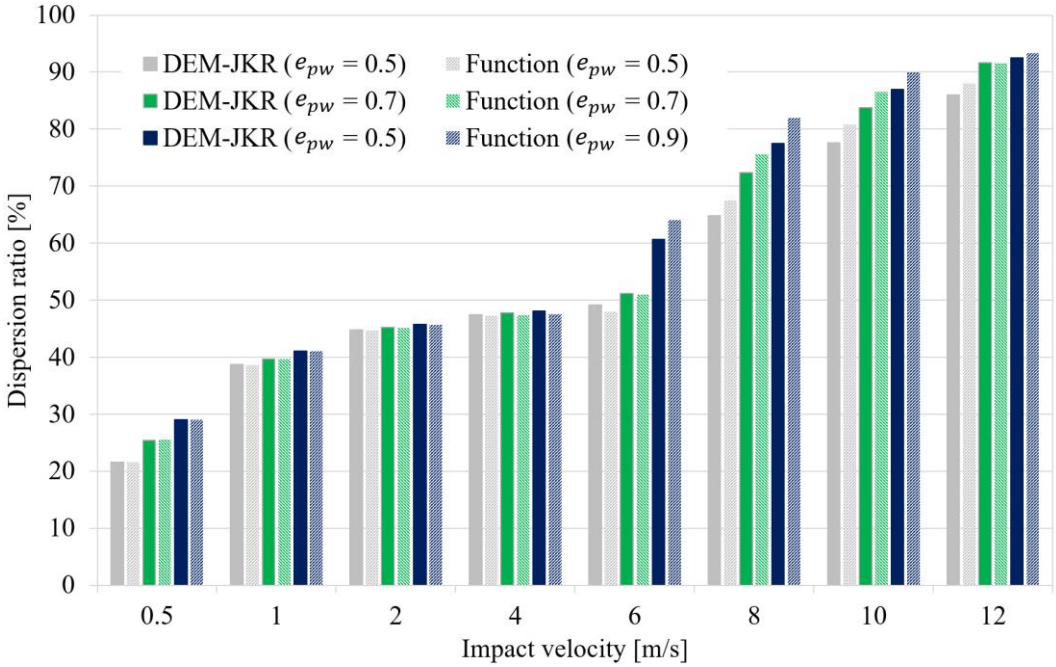

Figure 4: Comparison of the adhesive DEM-JKR simulations and the application of the dust detachment functions in terms of the dispersion ratio for the variation of the restitution coefficient e_{pw} during a straight, vertical bulk particle-wall impact.

Fig. 5 shows the results for varying impact angles at a constant restitution coefficient of e_{pw} = 0.7. Here, also a good agreement between the adhesive DEM-JKR and the realized dust detachment functions is visible. The lower the angle of impact, the lower the bulk particle velocity in the vertical direction towards the wall. This also leads to lower inertia forces and consequently to less dust dispersion.

Both examples show that the normal lift-off condition as well as the tangential lift-off condition can predict the dust dispersion of individual adhered dust particles during particle-wall contacts compared to much more computationally intensive adhesive DEM-JKR simulations. The detachment criteria should also be applicable to particle-particle contacts and particle-wall impacts under random carrier particle orientations by taking into account the rotation of the latter particle. It has to be kept in mind that by specifying a constant particle size, the effect of dust particle collisions on the carrier surface is almost excluded, which could lead to enhanced dust entrainment when a broader particle size distribution is considered. Such entrainment is currently yet not realized for in the dust release functions. Furthermore, for multiple contacts there could be additional deviations when using the derived dust release functions, since the acting inertia forces can change abruptly in the case of multiple contacts.

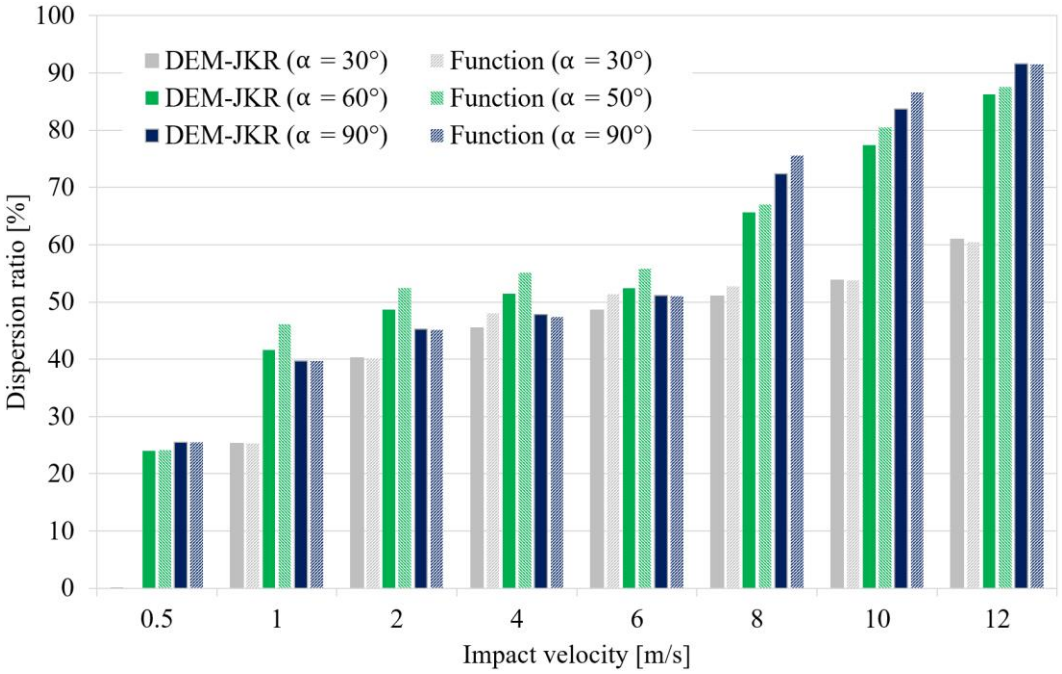

Figure 5: Comparison of the adhesive DEM-JKR simulations and the application of the dust detachment functions in terms of the dispersion ratio for the variation of the contact angle with a bulk particle-wall restitution coefficient of e_{pw} = 0.70 during a straight/oblique impact.

4 CONCLUSION

In addition to a lift-off condition in the normal direction, a novel tangential lift-off condition was derived for the prediction of the dust dispersion from a carrier surface. The performed adhesive DEM-JKR simulations and the application of the modified dust release functions

demonstrate that it is possible to calculate the physical dust detachment of adhering fine particles of constant size in the event of a bulk particle-wall impact. For the application of the dust release functions in the DEM, only the fixed positions of each adhering dust particle must be known, whereby it is possible to assume the surface texture for several bulk particles to be equal. The derived methodology allows to predict dust detachment of individual dust particles with significantly less computing time than by a DEM-JKR. As a next step, it is planned to validate obtained numerical results with experimental investigations. For this purpose, the adhering well-defined powder phase has to be analyzed before and after an impact in both experiment and simulation.

REFERENCES

[1] S. Chakravarty, M. Fischer, O. Le Bihan, M. Morgeneyer, Towards a theoretical understanding of dustiness, Granul. Matter. 21 (2019). doi:10.1007/s10035-019-0929-z.

[2] D. Schulz, N. Schwindt, E. Schmidt, R. Jasevičius, H. Kruggel-Emden, Investigation of the dust release from bulk material undergoing various mechanical processes using a coupled DEM/CFD approach, Powder Technol. 355 (2019) 37–56. doi:10.1016/j.powtec.2019.07.005.

[3] J.E. Hilton, P.W. Cleary, Dust modelling using a combined CFD and discrete element formulation, Int. J. Numer. Methods Fluids. 72 (2013) 528–549. doi:10.1002/fld.3750.

[4] Y. Cui, M. Sommerfeld, The modelling of carrier-wall collision with drug particle detachment for dry powder inhaler applications, Powder Technol. 344 (2019) 741–755. doi:10.1016/j.powtec.2018.12.067.

[5] K.L. Johnson, K. Kendall, A.D. Roberts, Surface energy and the contact of elastic solids, in: Proc. R. Soc. Lond. A 324, 1971: pp. 301–313. doi:10.1098/rspa.1971.0141.

[6] H.C. Hamaker, The London-van der Waals attraction between spherical particles, Physica. 4 (1937) 1058–1072. doi:10.1016/S0031-8914(37)80203-7.

[7] Y. Tsuji, T. Tanaka, T. Ishida, Lagrangian numerical simulation of plug flow of cohesionless particles in a horizontal pipe, Powder Technol. 71 (1992) 239–250. doi:10.1016/0032-5910(92)88030-L.

[8] R.D. Mindlin, Compliance of Elastic Bodies in Contact, J. Appl. Mech. 16 (1949) 259–268. doi:10.1115/1.4009973.

[9] A. Chokshi, A.G.G.M. Tielens, D. Hollenbach, Dust Coagulation, Astrophys. J. 407 (1993) 806–8019. doi:10.1086/172562.

[10] C. Thornton, Interparticle sliding in the presence of adhesion, J. Phys. D. Appl. Phys. 24 (1991) 1942–1946. doi:10.1088/0022-3727/24/11/007.

[11] C. Thornton, K.K. Yin, Impact of elastic spheres with and without adhesion, Powder Technol. 65 (1991) 153–166. doi:10.1016/0032-5910(91)80178-L.

[12] C. Dominik, A.G.G.M. Tielens, Resistance to rolling in the adhesive contact of two elastic spheres, Philos. Mag. A Phys. Condens. Matter, Struct. Defects Mech. Prop. 72 (1995) 783–803. doi:10.1080/01418619508243800.

[13] N. Woschny, D. Schulz, H. Kruggel-Emden, E. Schmidt, Ein experimentell-numerischer Ansatz zur Entwicklung von Staubfreisetzungsfunktionen, Chemie Ing. Tech. (2021). doi:10.1002/cite.202000191.

[14] Bergström L., Hamaker constants of inorganic materials, Adv. Colloid Interface Sci. 70 (1997) 125–169. doi:10.1016/S0001-8686(97)00003-1.

[15] J. Visser, On Hamaker constants: A comparison between Hamaker constants and Lifshitz-van der Waals constants, Adv. Colloid Interface Sci. 3 (1972) 331–363. doi:10.1016/0001-8686(72)85001-2.

[16] A.H. Ibrahim, P.F. Dunn, R.M. Brach, Microparticle detachment from surfaces exposed to turbulent air flow: controlled experiments and modeling, J. Aerosol Sci. 34 (2003) 765–782. doi:10.1016/S0021-8502(03)00031-4.